Electromagnetic Interference Analysis of Multiconductor Transmission Line Networks Using Longitudinal Partitioning-Based Waveform Relaxation Algorithm

Sourajeet Roy, *Student Member, IEEE*, Amir Beygi, and Anestis Dounavis, *Member, IEEE*

***Abstract*—With the use of low powered devices, susceptibility of high-speed interconnects to electromagnetic interference (EMI) is becoming a critical aspect of signal integrity analysis. For modeling the EMI in time domain, commercial circuit simulators like SPICE typically use longitudinal segmentation methodologies to discretize the interconnect network. For long lines as found in printed circuit board or cables, a large number of longitudinal segments are required to capture the response of the network leading to inefficient simulations. In this study, a waveform relaxation (WR) algorithm for the efficient EMI analysis of multiconductor transmission line networks is presented. Techniques to compress the size of the subcircuits, reduce communication overheads, and accelerate the convergence of the WR iterations are provided. The overall algorithm is demonstrated to be highly parallelizable and exhibits good scaling with both the size of the network involved and the number of central processing units available.**

***Index Terms*—Convergence analysis, delay, electromagnetic interference (EMI), incident fields, longitudinal partitioning, transient simulation, transmission line, waveform relaxation (WR).**

I. Introduction

With the constant increase in operating frequencies, interconnects need to be modeled as distributed multiconductor transmission lines (MTLs) for accurate signal integrity analysis of modern integrated circuits (IC) [1]. Moreover, with the increased use of low powered devices, susceptibility of interconnects at the chip, board, and packaging levels to incident electromagnetic (EM) fields has become a major reason behind signal degradation in high-speed packages [2]. As a result, efficient and accurate electromagnetic interference (EMI) analysis of large MTL networks has become necessary for modern design cycles.

Various time-domain macromodels have been reported in the literature [3]–[13] which are capable of performing EMI analysis of MTL networks using commercial circuit simulators with IC emphasis (like SPICE). However, macromodeling techniques for large distributed networks may require significant central processing unit (CPU) time and memory, thereby making them computationally prohibitive for fast EMI analysis.

The waveform relaxation (WR) algorithm, since its introduction [14], has emerged as an attractive technique to reduce the simulation costs of large networks [15]–[27]. WR algorithms attempt to partition the network into smaller subcircuits where the couplings between the subcircuits are preserved using time-domain sources introduced within each subcircuit, referred to as relaxation sources. These subcircuits can be solved concurrently using traditional iterative techniques leading to a smaller overall computational cost than the original network. Presently, two approaches exist for an application of WR to transmission line networks. One such approach is the transverse partitioning scheme (TP-WR) [16]–[20] where the MTLs are partitioned into single lines by assuming weak capacitive and inductive coupling between the lines.

An alternative approach toward WR algorithms is based on longitudinal partitioning (LP) of the network into subcircuits [21]–[27]. While longitudinal partitioning schemes based on the generalized method of characteristics (MoC) have been reported in [21]–[25], more recent works [26] have focused on partitioning the line based on segmentation models such as the conventional resistive-inductive-conductive-capacitive (RLGC) lumped model. However, partitioning techniques based on segmentation models have a common limitation that since each segment is cascaded with the next, the Dirichlets transmission condition is required to preserve the current/voltage waveform at the boundary of the subcircuits and consequently leads to slow convergence of the WR iterations [26]. The work in [26] accelerated the convergence of the WR algorithm by artificially exchanging additional voltage/current waveforms (i.e., increasing the overlap between subcircuits) followed by optimization routines.

More recently, in [27], an LP-WR algorithm based on the delay extraction-based passive compact transmission line (DEPACT) segmentation model [28], [29] was presented for transmission line networks. The DEPACT model represents

Manuscript received February 3, 2012; revised April 5, 2012; accepted May 17, 2012. Date of publication September 21, 2012; date of current version April 11, 2013. This work was supported in part by the Natural Sciences and Engineering Research Council of Canada, in part by the Canada Foundation for Innovation, in part by the Canadian Microelectronics Corporation, and in part by the Ministry of Research and Innovation—Early Research Award.

S. Roy and A. Dounavis are with the Department of Electrical and Computer Engineering, Western University, London, ON N6A 5B9, Canada (e-mail: sroy33@uwo.ca; adounavis@eng,uwo.ca).

A. Beygi is with Evertz Microsystems, Burlington, ON L7L 5Z9, Canada (e-mail: abeygi@uwo.ca).

Color versions of one or more of the figures in this paper are available online at http://ieeexplore.ieee.org.

Digital Object Identifier 10.1109/TEMC.2012.2216511

lossy transmission lines as a cascade of lumped circuit elements alternating with lossless line sections where the lossless line sections are realized in the time domain using the MoC [30]. Partitioning the network at the natural interfaces provided by the MoC rather than between two successive DEPACT segments avoids the need to preserve the continuity of the voltage/current waveforms at the subcircuit boundary (Dirichlet's transmission conditions) and is shown to provide efficient convergence for transmission line problems [27].

This study extends the concepts in [27] to perform efficient EMI analysis of MTL networks. The distributed nature of the incident field coupling with the network is represented as lumped sources introduced into each DEPACT section. Combining the lumped sources (due to EM fields) with the delayed sources due to the MoC representation of the lossless section leads to a more compact realization of the subcircuits as well as reduces the communication overhead between processors leading to a more scalable LP-WR algorithm. The resultant subcircuits are solved independently using a hybrid iterative technique that combines the complimentary features of Gauss Seidel (GS) and the Gauss Jacobi (GJ) techniques. This hybrid technique exhibits superior convergence properties when compared to the traditional GJ algorithm while maintaining its high parallelizability with respect to the number of CPUs available. Moreover, a methodology to provide an improved guess of the relaxation sources based on the delay extraction feature of DEPACT is used to further speed up the convergence. The overall algorithm is highly parallelizable and exhibits good scaling with both the size of the circuit involved and the number of CPUs available as illustrated in Section IV.

II. EMI Analysis of MTL Structures

In order to explain the contributions of the proposed work, this section discusses the general formulation of MTL structures exposed to incident fields followed by a description of the DEPACT macromodel reported in [13] to perform the EMI analysis in the frequency domain.

A. General Formulation of MTLs Exposed to Incident Fields

Consider an MTL network supporting quasi-transverse electromagnetic mode of propagation, backed by a reference plane and exposed to incident fields as shown in Fig. 1. In such cases, the MTL structure is described by the inhomogeneous Telegrapher's partial differential equations as follows [2], [10]–[13]:

$$\frac{\partial}{\partial x}\begin{bmatrix}\boldsymbol{V}(z,s)\\ -\boldsymbol{I}(z,s)\end{bmatrix}=\begin{bmatrix}\mathbf{0} & -(\boldsymbol{R}(s)+s\boldsymbol{L}(s))\\ -(\boldsymbol{G}(s)+s\boldsymbol{C}(s)) & \mathbf{0}\end{bmatrix}\times\begin{bmatrix}\boldsymbol{V}(z,s)\\ \boldsymbol{I}(z,s)\end{bmatrix}+\begin{bmatrix}\boldsymbol{V}_F(z,s)\\ \boldsymbol{I}_F(z,s)\end{bmatrix} \quad (1)$$

where $\boldsymbol{V}(z,s)$ and $\boldsymbol{I}(z,s)$ represent the spatial distribution of the voltage and current along the longitudinal direction, $\boldsymbol{R}(s)$, $\boldsymbol{L}(s)$, $\boldsymbol{G}(s)$, and $\boldsymbol{C}(s)$ are the frequency-dependent resistive, inductive, conductive, and capacitive per-unit-length (p.u.l.) parameters of the line respectively, $s=j2\pi f$ is the Laplace variable, and f is the instantaneous frequency. The p.u.l. parameter matrices

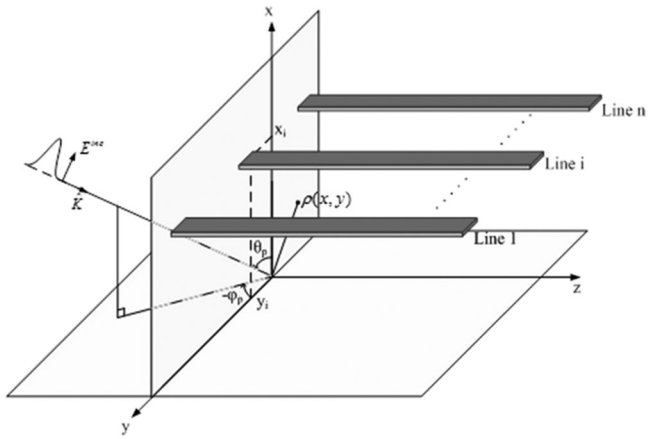

Fig. 1. Geometry of an MTL exposed to an incident field.

can be obtained from a static solution of the Laplace equation in the 2-D plane containing the cross section of the conductors of Fig. 1 [2]. The functions $\boldsymbol{V}_F(z,s)$ and $\boldsymbol{I}_F(z,s)$ represent the effect of the incident field coupled to the MTL and can be mathematically expressed as

$$\begin{aligned}\boldsymbol{V}_F(z,s)&=-\frac{\partial}{\partial z}\boldsymbol{E}_T(z,s)+\boldsymbol{E}_L(z,s)\\ \boldsymbol{I}_F(z,s)&=-\left(\boldsymbol{G}(s)+s\boldsymbol{C}(s)\right)\boldsymbol{E}_T(z,s)\end{aligned} \quad (2)$$

and

$$\begin{aligned}\boldsymbol{E}_L(z,s)&=\left(\vec{\varepsilon}_z(x_i,y_i,z)-\vec{\varepsilon}_z(x_0,y_0,z)\right)\\ \boldsymbol{E}_T(z,s)&=\int_{\rho(x,y)}\vec{\varepsilon}_t(\rho,z)\cdot d\rho.\end{aligned} \quad (3)$$

The variables $\vec{\varepsilon}_z$ and $\vec{\varepsilon}_t$ are the longitudinal and transverse components of the incident electric field; (x_i,y_i) and (x_0,y_0) refer to spatial coordinates of the ith conductor and the reference conductor, respectively, and ρ is a parameter of x and y in the transverse plane (see Fig. 1).

Different types of far radiating sources are often approximated in a localized region of space as uniform plane waves [2], [10]–[13]. For such examples, the electric field of the incident field can be expressed as

$$\vec{E}^i(x,y,z)=E(s)(A_x\vec{a}_x+A_y\vec{a}_y+A_z\vec{a}_z)e^{-s\beta_x x}e^{-s\beta_y y}e^{-s\beta_z z} \quad (4)$$

where $E(s)$ is the electric field amplitude, A_x, A_y, and A_z are the direction cosines of the incoming wave, and $\beta=[\beta_x\ \ \beta_y\ \ \beta_z]^T$ is the propagation vector. Replacing (4) into (3) and solving (1), the frequency-domain expression of the current/voltage at the line extremities is written [13] as

$$\left(\begin{bmatrix}\boldsymbol{V}(l,s)\\ -\boldsymbol{I}(l,s)\end{bmatrix}-\begin{bmatrix}\boldsymbol{V}_t(l,s)\\ \mathbf{0}\end{bmatrix}\right)=e^{\boldsymbol{\Phi}l}\times\left(\begin{bmatrix}\boldsymbol{V}(0,s)\\ \boldsymbol{I}(0,s)\end{bmatrix}-\begin{bmatrix}\boldsymbol{V}_t(0,s)\\ \mathbf{0}\end{bmatrix}\right)+\boldsymbol{J}(l,s) \quad (5)$$

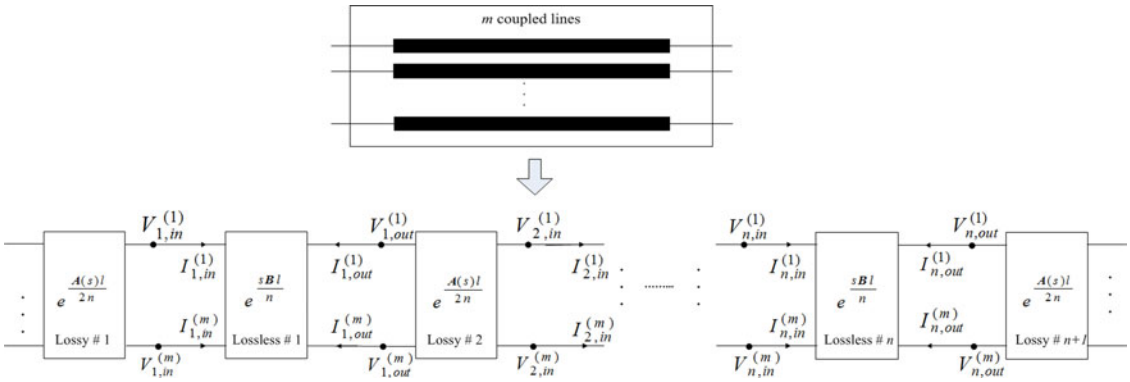

Fig. 2. Discretization of an MTL using DEPACT (without incident fields).

where

$$\boldsymbol{\Phi} = \boldsymbol{A} + s\boldsymbol{B}$$

$$\boldsymbol{A} = \begin{bmatrix} \boldsymbol{0} & -\boldsymbol{R}(s) - s(\boldsymbol{L}(s) - \boldsymbol{L}_\infty) \\ -\boldsymbol{G}(s) - s(\boldsymbol{C}(s) - \boldsymbol{C}_\infty) & \boldsymbol{0} \end{bmatrix}$$

$$\boldsymbol{B} = \begin{bmatrix} \boldsymbol{0} & -\boldsymbol{L}_\infty \\ -\boldsymbol{C}_\infty & \boldsymbol{0} \end{bmatrix} \tag{6}$$

and

$$\boldsymbol{J}(l,s) = \int_0^l e^{\boldsymbol{\Phi}(l-z)} \begin{bmatrix} \boldsymbol{V}_z(z,s) \\ \boldsymbol{0} \end{bmatrix} dz. \tag{7}$$

In (6), the matrices $\boldsymbol{L}_\infty$ and $\boldsymbol{C}_\infty$ are the values of the inductive and capacitive p.u.l. parameters at the maximum frequency of interest $s_\infty = j2\pi f_{\max}$, respectively. Moreover, the terms $\boldsymbol{V}_t$ and $\boldsymbol{V}_z$ can be expressed in closed form as

$$\boldsymbol{V}_z(z,s) = se^{-s\beta_z z} E_0(s)\boldsymbol{V}_{F1}; \quad \boldsymbol{V}_t(z,s) = e^{-s\beta_z z} E_0(s)\boldsymbol{V}_{F2} \tag{8}$$

where

$$\boldsymbol{V}_{F1} = \begin{bmatrix} \vdots \\ -2A_z\beta_y y_i \\ \vdots \end{bmatrix}; \quad \boldsymbol{V}_{F2} = \begin{bmatrix} \vdots \\ -2A_x x_i \\ \vdots \end{bmatrix}. \tag{9}$$

In order to represent the EMI effects of (5) using an equivalent circuit model, the DEPACT macromodel of [28] is utilized as explained in the next section.

B. DEPACT Macromodel for EMI Analysis

The DEPACT macromodel uses a modified Lie product [31] to approximate the exponential function $e^{\boldsymbol{\Phi}l} = e^{(\boldsymbol{A}+s\boldsymbol{B})l}$ in (5) as a product of exponentials as

$$e^{(\boldsymbol{A}+s\boldsymbol{B})l} \approx \prod_{i=1}^{n} \boldsymbol{\Psi}_i + \varepsilon_n \text{ and } \boldsymbol{\Psi}_i = e^{\frac{\boldsymbol{A}l}{2n}} e^{\frac{s\boldsymbol{B}l}{n}} e^{\frac{\boldsymbol{A}l}{2n}} \tag{10}$$

where "n" is the number of segments and $\boldsymbol{\Psi}_i$ represents the ith DEPACT segment. Equation (10) translates to the MTL (without incident fields) being discretized into a cascade of alternating subsections with the individual stamps of $e^{\boldsymbol{A}l/2n}$ (lossy section) and $e^{s\boldsymbol{B}/n}$ (lossless section) as illustrated in Fig. 2 [28]. The number of DEPACT sections "n" is chosen to be sufficiently large for the modified Lie product to accurately match the exponential solution of Telegrapher's differential equations in (10) over the bandwidth of $f_{\max}$. Further discussion on the choice of n is provided in [28]. Details regarding the SPICE modeling of the lossy $(e^{\boldsymbol{A}l/2n})$ and lossless sections $(e^{s\boldsymbol{B}l/n})$ are provided in [29].

The effect of the incident field coupling to the MTL structure of Fig. 2 can be reduced to applying (1) to each DEPACT segment $\boldsymbol{\Psi}_i$ in a piecewise manner. For this purpose, the effect of the incident field on the lossless sections $(e^{s\boldsymbol{B}l/n})$ is evaluated first. Thereafter, to consider the effect of the line losses, the lossy sections $(e^{\boldsymbol{A}l/2n})$ are incorporated into the macromodel [13]. For this purpose, the solution of (1) for any ith lossless section of Fig. 2 can be formulated similar to (5)–(7) [13]

$$\left(\begin{bmatrix} \boldsymbol{V}_{i,\text{out}}(s) \\ -\boldsymbol{I}_{i,\text{out}}(s) \end{bmatrix} - \begin{bmatrix} \boldsymbol{V}_t(z_i,s) \\ \boldsymbol{0} \end{bmatrix} \right) = e^{\frac{s\boldsymbol{B}l}{n}} \left(\begin{bmatrix} \boldsymbol{V}_{i,\text{in}}(s) \\ \boldsymbol{I}_{i,\text{in}}(s) \end{bmatrix} - \begin{bmatrix} \boldsymbol{V}_t(z_{i-1},s) \\ \boldsymbol{0} \end{bmatrix} \right) + \boldsymbol{J}_i(s) \tag{11}$$

where

$$\boldsymbol{J}_i(s) = \int_{z_{i-1}}^{z_i} e^{s\boldsymbol{B}(z_i - z)} \begin{bmatrix} \boldsymbol{V}_z(z,s) \\ \boldsymbol{0} \end{bmatrix} dz$$

$$\boldsymbol{V}_{i,\text{in}}(s) = [V_{i,\text{in}}^{(1)}(s), ..., V_{i,\text{in}}^{(m)}(s)]^t$$

$$\boldsymbol{V}_{i,\text{out}}(s) = [V_{i,\text{out}}^{(1)}(s), ..., V_{i,\text{out}}^{(m)}(s)]^t$$

$$\boldsymbol{I}_{i,\text{in}}(s) = [I_{i,\text{in}}^{(1)}(s), ..., I_{i,\text{in}}^{(m)}(s)]^t$$

$$\boldsymbol{I}_{i,\text{out}}(s) = [I_{i,\text{out}}^{(1)}(s), ..., I_{i,\text{out}}^{(m)}(s)]^t. \tag{12}$$

The variables $\boldsymbol{V}_{i,\text{in}}(s)$, $\boldsymbol{I}_{i,\text{in}}(s)$ and $\boldsymbol{V}_{i,\text{out}}(s)$, $\boldsymbol{I}_{i,\text{out}}(s)$ represent the near- and far-end voltage and current sources for any ith lossless section of Fig. 2, respectively, where the superscript represents the line number and $z_{i-1} = (i-1)l/n$. For the case of lossless MTL, the integral of (12) can be solved in closed form [13] and when replaced back in (11) yields the frequency-domain solution for the lossless MTLs exposed to incident fields as

$$\begin{bmatrix} \tilde{\boldsymbol{V}}_{i,\text{out}}(s) \\ -\tilde{\boldsymbol{I}}_{i,\text{out}}(s) \end{bmatrix} = e^{\frac{s\boldsymbol{B}l}{n}} \begin{bmatrix} \tilde{\boldsymbol{V}}_{i,\text{in}}(s) \\ \tilde{\boldsymbol{I}}_{i,\text{in}}(s) \end{bmatrix} \tag{13}$$

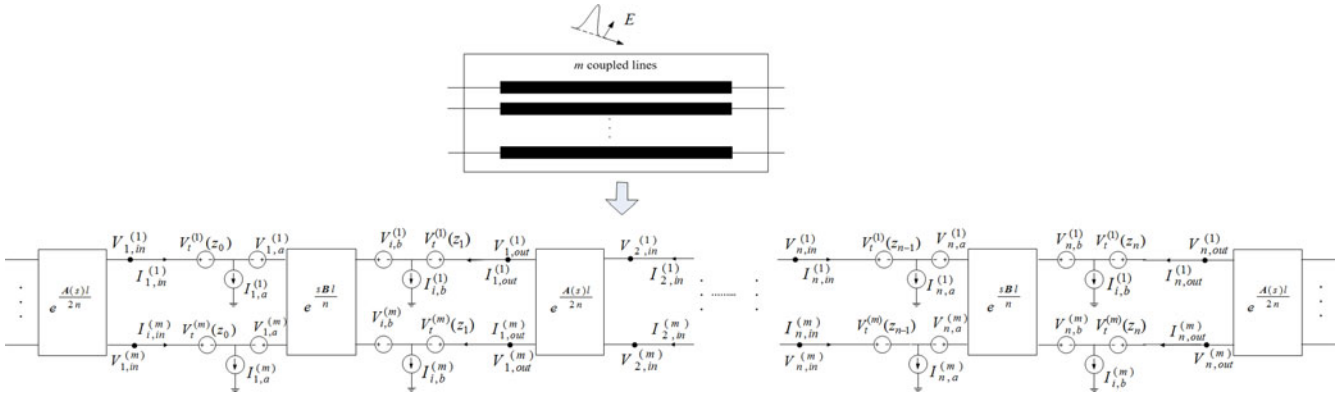

Fig. 3. Discretization of an MTL using DEPACT in the presence of incident fields.

where

$$\tilde{\boldsymbol{V}}_{i,\text{in}}(s) = \boldsymbol{V}_{i,\text{in}}(s) - (\boldsymbol{V}_t(z_{i-1},s) - \boldsymbol{V}_{i,a}(s))$$
$$\tilde{\boldsymbol{I}}_{i,\text{in}}(s) = \boldsymbol{I}_{i,\text{in}}(s) + \boldsymbol{I}_{i,a}(s)$$
$$\tilde{\boldsymbol{V}}_{i,\text{out}}(s) = \boldsymbol{V}_{i,\text{out}}(s) - (\boldsymbol{V}_t(z_i,s) - \boldsymbol{V}_{i,b}(s))$$
$$\tilde{\boldsymbol{I}}_{i,\text{out}}(s) = \boldsymbol{I}_{i,\text{out}}(s) - \boldsymbol{I}_{i,b}(s),\ i = 1,2,\ldots,n \quad (14)$$

$$\begin{bmatrix} \boldsymbol{V}_{i,a}(s) \\ \boldsymbol{I}_{i,a}(s) \end{bmatrix} = e^{-s\beta_s z_{i-1}} E_0(s) \begin{bmatrix} \beta_z \boldsymbol{I} & -\boldsymbol{L}_\infty \\ -\boldsymbol{C}_\infty & \beta_z \boldsymbol{I} \end{bmatrix}^{-1} \begin{bmatrix} \boldsymbol{V}_{F1} \\ \boldsymbol{0} \end{bmatrix}$$

$$\begin{bmatrix} \boldsymbol{V}_{i,b}(s) \\ \boldsymbol{I}_{i,b}(s) \end{bmatrix} = e^{-s\beta_s z_i} E_0(s) \begin{bmatrix} \beta_z \boldsymbol{I} & -\boldsymbol{L}_\infty \\ -\boldsymbol{C}_\infty & \beta_z \boldsymbol{I} \end{bmatrix}^{-1} \begin{bmatrix} \boldsymbol{V}_{F1} \\ \boldsymbol{0} \end{bmatrix}. \quad (15)$$

Considering the line losses, the lossy sections $(e^{\boldsymbol{A}l/2n})$ are incorporated between successive lossless sections to provide the equivalent circuit model for the entire MTL structure in the presence of incident fields as illustrated in Fig. 3.

It is appreciated that the solution of the macromodel of Fig. 3 requires the inversion of the corresponding modified nodal analysis (MNA) matrix. The computational complexity of directly inverting a matrix scales to $O(n^3)$ [32], [33]. However, the matrices obtained by traditional circuit simulators are sparse by nature and can be solved more efficiently using sparse matrix routines at a cost of $O(n^\alpha)$ where typically $1.5 \leq \alpha \leq 2$ depending on the sparsity of the matrix [16]. For large distributed networks, DEPACT macromodel of Fig. 3 may require many segments for the accurate approximation of (10). For such cases, the superlinear scaling of the computational cost for traditional circuit simulators is a major factor limiting their applicability. To address the aforementioned issue, the proposed contribution of applying the LP-WR algorithm [27] to perform EMI analysis is explained in the following section.

III. Development of the Proposed LP-WR for EMI Analysis

This section begins by describing the methodology to longitudinally partition the DEPACT macromodel introduced in Section II into compact subcircuits for transient analysis followed by the iterative techniques to solve the subcircuits.

A. Generating Compact Subcircuits

In [13], a similarity transform is directly performed on (13) to decouple the m coupled lossless MTL into m single lossless lines. In this study, the similarity transform of [13] is modified in order to group the lumped sources due to the incident fields with the delayed sources due to the MoC which leads to a more scalable LP-WR algorithm. For this purpose, the proposed transformation is performed on the quantities $\boldsymbol{V}_{i,\text{in}}(s)$, $\boldsymbol{I}_{i,\text{in}}(s)$, $\boldsymbol{V}_{i,\text{out}}(s)$, $\boldsymbol{I}_{i,\text{out}}(s)$ (and not on $\tilde{\boldsymbol{V}}_{i,\text{in}}(s), \tilde{\boldsymbol{I}}_{i,\text{in}}(s), \tilde{\boldsymbol{V}}_{i,\text{out}}(s), \tilde{\boldsymbol{I}}_{i,\text{out}}(s)$) as

$$\boldsymbol{V}_{i,\text{in}}(s) = \boldsymbol{T}_V \bar{\boldsymbol{V}}_{i,\text{in}}(s); \quad \boldsymbol{I}_{i,\text{in}}(s) = \boldsymbol{T}_I \bar{\boldsymbol{I}}_{i,\text{in}}(s)$$
$$\boldsymbol{V}_{i,\text{out}}(s) = \boldsymbol{T}_V \bar{\boldsymbol{V}}_{i,\text{out}}(s); \quad \boldsymbol{I}_{i,\text{out}}(s) = \boldsymbol{T}_I \bar{\boldsymbol{I}}_{i,\text{out}}(s) \quad (16)$$

where the matrices $\boldsymbol{T}_V$ and $\boldsymbol{T}_I$ are constant matrices chosen to diagonalize $\boldsymbol{L}_\infty$ and $\boldsymbol{C}_\infty$ and have the following properties [2]:

$$\tilde{\boldsymbol{L}} = \boldsymbol{T}_V^{-1} \boldsymbol{L}_\infty \boldsymbol{T}_I; \quad \tilde{\boldsymbol{C}} = \boldsymbol{T}_I^{-1} \boldsymbol{C}_\infty \boldsymbol{T}_V; \quad \boldsymbol{T}_V^t = \boldsymbol{T}_I^{-1}. \quad (17)$$

Here $\tilde{\boldsymbol{L}} = \text{diag}\{l_1, l_2, \ldots, l_m\}$ and $\tilde{\boldsymbol{C}} = \text{diag}\{c_1, c_2, \ldots, c_m\}$ are diagonal matrices and the superscript "t" denotes the transpose of the matrix. Replacing (16) into (13) and converting to time domain yields the following m decoupled MoC equations:

$$\hat{\boldsymbol{V}}_{i,\text{in}}(t) = \boldsymbol{Z}_0 \hat{\boldsymbol{I}}_{i,\text{in}}(t) + \boldsymbol{W}_{2i-1}(t)$$
$$\hat{\boldsymbol{V}}_{i,\text{out}}(t) = \boldsymbol{Z}_0 \hat{\boldsymbol{I}}_{i,\text{out}}(t) + \boldsymbol{W}_{2i}(t), i = 1,2,\ldots,n \quad (18)$$

where

$$\boldsymbol{W}_{2i-1}(t) = [W_{2i-1}^{(1)}(t), \ldots, W_{2i-1}^{(m)}(t)]^t$$
$$\boldsymbol{W}_{2i}(t) = [W_{2i}^{(1)}(t), \ldots, W_{2i}^{(m)}(t)]^t$$
$$\boldsymbol{Z}_0 = [Z_0^{(1)}, \ldots, Z_0^{(m)}]^t$$
$$W_{2i-1}^{(j)}(t) = 2\hat{V}_{i,\text{out}}^{(j)}(t-\tau_j) - W_{2i}^{(j)}(t-\tau_j)$$
$$W_{2i}^{(j)}(t) = 2\hat{V}_{i,\text{in}}^{(j)}(t-\tau_j) - W_{2i-1}^{(j)}(t-\tau_j),\ j = 1,\ldots,m \quad (19)$$

$$\hat{\boldsymbol{V}}_{i,\text{in}}(t) = \bar{\boldsymbol{V}}_{i,\text{in}}(t) - \boldsymbol{T}_V^{-1}(\boldsymbol{V}_t(z_{i-1},t) - \boldsymbol{V}_{i,a}(t))$$
$$\hat{\boldsymbol{I}}_{i,\text{in}}(t) = \bar{\boldsymbol{I}}_{i,\text{in}}(t) + \boldsymbol{T}_I^{-1} \boldsymbol{I}_{i,a}(t)$$

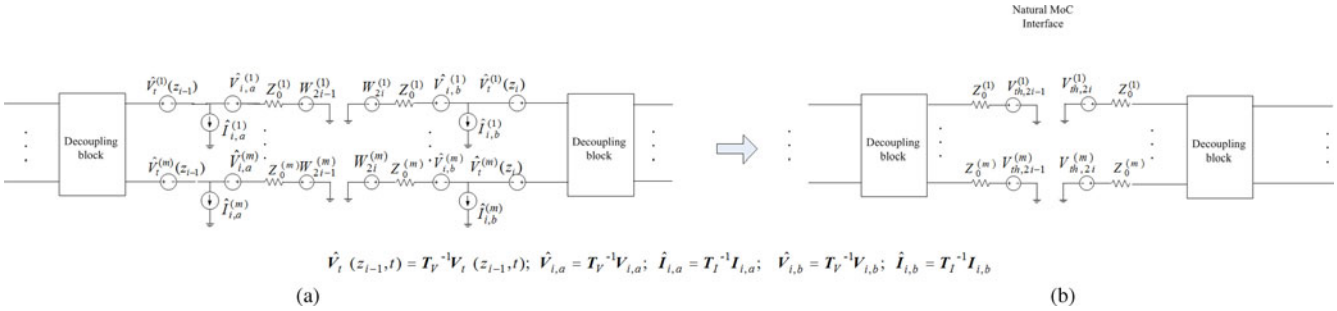

Fig. 4. Proposed circuit representation of the incident field coupled with ith lossless section. (a) Prior to grouping of the lumped sources. (b) After grouping of the lumped sources using (25).

$$\hat{\boldsymbol{V}}_{i,\text{out}}(t) = \bar{\boldsymbol{V}}_{i,\text{out}}(t) - \boldsymbol{T}_V^{-1}(\boldsymbol{V}_t(z_i,t) - \boldsymbol{V}_{i,b}(t))$$
$$\hat{\boldsymbol{I}}_{i,\text{out}}(t) = \bar{\boldsymbol{I}}_{i,\text{out}}(t) - \boldsymbol{T}_I^{-1}\boldsymbol{I}_{i,b}(t), i = 1,2,...,n. \quad (20)$$

The superscript "j" represents the line number, and $Z_0^{(j)} = \sqrt{l_j/c_j}$ and $\tau_j = l\sqrt{l_j c_j}/n$ represent the characteristic impedance and delay of each lossless section, respectively, of the jth line. The variables $\bar{\boldsymbol{V}}_{i,\text{in}}(t), \bar{\boldsymbol{I}}_{i,\text{in}}(t), \bar{\boldsymbol{V}}_{i,\text{out}}(t), \bar{\boldsymbol{I}}_{i,\text{out}}(t)$ and $\boldsymbol{V}_{i,a}(t)$, $\boldsymbol{I}_{i,a}(t)$, $\boldsymbol{V}_{i,b}(t)$, $\boldsymbol{I}_{i,b}(t)$, $\boldsymbol{V}_t(z_{i-1},t)$ are simply the time-domain waveforms of the corresponding sources in (16) and (14), respectively. The lumped sources $\boldsymbol{V}_{i,a}(t), \boldsymbol{I}_{i,a}(t), \boldsymbol{V}_{i,b}(t), \boldsymbol{I}_{i,b}(t)$, and $\boldsymbol{V}_t(z_{i-1},t)$ can be obtained in a closed-form manner using the direct inverse Laplace transform of (15) and (8) as [13]

$$\begin{bmatrix} \boldsymbol{V}_{i,a}(t) \\ \boldsymbol{I}_{i,a}(t) \end{bmatrix} = E_0(t-\beta_z z_{i-1}) \begin{bmatrix} \beta_z \boldsymbol{I} & -\boldsymbol{L}_\infty \\ -\boldsymbol{C}_\infty & \beta_z \boldsymbol{I} \end{bmatrix}^{-1} \begin{bmatrix} \boldsymbol{V}_{F1} \\ \boldsymbol{0} \end{bmatrix}$$
$$\begin{bmatrix} \boldsymbol{V}_{i,b}(t) \\ \boldsymbol{I}_{i,b}(t) \end{bmatrix} = E_0(t-\beta_z z_i) \begin{bmatrix} \beta_z \boldsymbol{I} & -\boldsymbol{L}_\infty \\ -\boldsymbol{C}_\infty & \beta_z \boldsymbol{I} \end{bmatrix}^{-1} \begin{bmatrix} \boldsymbol{V}_{F1} \\ \boldsymbol{0} \end{bmatrix}$$
$$\boldsymbol{V}_t(z_i,t) = E_0(t-\beta_z z_i)\boldsymbol{V}_{F2}. \quad (21)$$

Based on (18)–(21), the representation of the ith lossless section of Fig. 3 is illustrated in Fig. 4(a). In Fig. 4(a) the "decoupling block" represents the lumped dependent sources used to represent the transformation of (16). A key feature of the proposed representation of Fig. 4(a) is that the lumped sources due to the incident fields $\boldsymbol{V}_{i,a}(t), \boldsymbol{I}_{i,a}(t), \boldsymbol{V}_{i,b}(t), \boldsymbol{I}_{i,b}(t), \boldsymbol{V}_{i,t}^{\text{inc}}(t)$ can be grouped together with $\boldsymbol{W}_{2i-1}(t), \boldsymbol{W}_{2i}(t)$ into a compact Thevenin's network as

$$\boldsymbol{V}_{\text{th},2i-1}(t) = \boldsymbol{T}_V^{-1}(\boldsymbol{V}_t(z_{i-1},t) - \boldsymbol{V}_{i,a}(t)) + \boldsymbol{Z}_0\boldsymbol{T}_I^{-1}\boldsymbol{I}_{i,a}(t) + \boldsymbol{W}_{2i-1}(t)$$
$$\boldsymbol{V}_{\text{th},2i}(t) = \boldsymbol{T}_V^{-1}(\boldsymbol{V}_t(z_i,t) - \boldsymbol{V}_{i,b}(t)) - \boldsymbol{Z}_0\boldsymbol{T}_I^{-1}\boldsymbol{I}_{i,b}(t) + \boldsymbol{W}_{2i}(t)$$
$$\boldsymbol{R}_{\text{th},2i-1} = \boldsymbol{R}_{\text{th},2i-1} = \boldsymbol{Z}_0 \quad (22)$$

where $\boldsymbol{V}_{\text{th},2i-1}(t), \boldsymbol{V}_{\text{th},2i}(t)$ represent Thevenin's equivalent sources and $\boldsymbol{R}_{\text{th},2i-1}(t), \boldsymbol{R}_{\text{th},2i}(t)$ represent Thevenin's equivalent impedance for the ith lossless section as displayed in Fig. 4(b). Replacing the expression for $\boldsymbol{W}_{2i-1}(t), \boldsymbol{W}_{2i}(t)$ from (19) into (22), Thevenin's sources can be rewritten using delay linear equations for each decoupled line as

$$V_{\text{th},2i-1}^{(j)}(t) = 2\bar{V}_{i,\text{out}}^{(j)}(t-\tau_j) - W_{2i}^{(j)}(t-\tau_j) + V_{2i-1,x}^{(j)}(t)$$
$$V_{\text{th},2i}^{(j)}(t) = 2\bar{V}_{i,\text{in}}^{(j)}(t-\tau_j) - W_{2i-1}^{(j)}(t-\tau_j) - V_{2i,x}^{(j)}(t), \quad j = 1,...,m \quad (23)$$

where

$$V_{2i-1,x}^{(j)}(t) = Z_0^{(j)}\left[\boldsymbol{T}_I^{-1}\right]_j I_{i,a}^{(j)}(t) + \left[\boldsymbol{T}_V^{-1}\right]_j \times (V_t^{(j)}(z_{i-1},t) - 2V_t^{(j)}(z_{i-1},t-2\tau_j)) - \left[\boldsymbol{T}_V^{-1}\right]_j (V_{i,a}^{(j)}(t) - 2V_{i,a}^{(j)}(t-2\tau_j))$$
$$V_{2i,x}^{(j)}(t) = Z_0^{(j)}\left[\boldsymbol{T}_I^{-1}\right]_j I_{i,b}^{(j)}(t) + \left[\boldsymbol{T}_V^{-1}\right]_j \times (V_t^{(j)}(z_i,t) - V_{i,b}^{(j)}(t)) \quad (24)$$

where $[\boldsymbol{A}]_j$ represents the jth row vector of $\boldsymbol{A}$. It is noted that the terms $V_{2i-1,x}^{(j)}, V_{2i,x}^{(j)}$ of (24) can be calculated offline and stored prior to the LP-WR iterations.

From Fig. 4(b), it is observed that each lossless section provides a natural MoC interfaces (disjoin) across which current/voltage information is exchanged using the delayed linear equations of (23). Partitioning the MTL macromodel of Fig. 4(b) along these natural MoC interfaces avoids the need of preserving the current/voltage continuity between subcircuits using Dirichlets transmission conditions and has been demonstrated to exhibit fast convergence for MTL networks in the absence of incident fields [27]. Extending such a partitioning methodology for EMI analysis of MTLs based on the proposed representation of Fig. 4(b) leads to n subcircuits where the sources $\boldsymbol{V}_{\text{th},2i-1}(t), \boldsymbol{V}_{\text{th},2i}(t)$ act as the relaxation sources responsible for maintaining the coupling between subcircuits.

It is observed that based on (22) the size of the MNA matrices of each subcircuits is reduced by eliminating the variables $\boldsymbol{V}_{i,a}(t), \boldsymbol{V}_{i,b}(t), \boldsymbol{I}_{i,a}(t), \boldsymbol{I}_{i,b}(t)$ [see Fig. 4(a) and (b)] thereby leading to more compact formulation of the subcircuits. Moreover, solution of each subcircuit using (22) now requires the prior knowledge of only the $2m$ waveforms $(\boldsymbol{V}_{\text{th},2i-2}(t), \boldsymbol{V}_{\text{th},2i-1}(t))$ rather than the $5m$ waveforms of $\boldsymbol{V}_{i-1,a}(t)$, $\boldsymbol{I}_{i-1,a}(t)$, $\boldsymbol{V}_t(z_{i-1},t)$, $\boldsymbol{W}_{2i-2}(t)$, $\boldsymbol{W}_{2i-1}(t)$ as would be required if the proposed partitioning scheme was directly applied to the circuit model of Fig. 3. The combination of

the aforementioned factors leads to improved scalability of the proposed LP-WR algorithm.

B. Hybrid Iterative Solution of Subcircuits for EMI Analysis

Once the network has been partitioned into subcircuits as shown in Fig. 4(b), various iterative techniques can be employed to solve the subcircuits in parallel [15]. In [27], a hybrid iterative technique was proposed which combined the complimentary features of both GS and GJ iterative techniques. In this paper, the hybrid technique has been extended to perform the WR iterations on the subcircuits obtained from the longitudinal partitioning in Section III-A.

To explain this technique, the n subcircuits are divided among two groups—group A containing the odd numbered subcircuits and group B, the even numbered subcircuits where the total number of subcircuits within each group is defined as

$$n_{\rm odd} = [n/2] \ - \ \text{group A}$$
$$n_{\rm even} = n - [n/2] \ - \ \text{group B} \tag{25}$$

and [.] represents the modulus function. Hereafter, the hybrid technique uses a nested iterative methodology to solve the subcircuits. The outer iteration solves groups A and B in sequence (using GS) with updating the relaxation sources after every group solution while the inner iteration solves the subcircuits within each group in parallel (using GJ).

To begin the iterations, an initial guess is chosen for the waveforms $\{\boldsymbol{V}^{(0)}_{{\rm th},4i-4}(t), \boldsymbol{V}^{(0)}_{{\rm th},4i-3}(t)\}, i = 1, 2, ..., n_{\rm odd}$, which are responsible for exciting only the odd numbered subcircuits (group A) where the superscripts for the aforementioned vectors represent the iteration count. The known waveforms of $\{\boldsymbol{V}^{(0)}_{{\rm th},4i-4}(t),\ \boldsymbol{V}^{(0)}_{{\rm th},4i-3}(t)\}$ translate to the following terminal conditions for the ith subcircuit in group A:

$$\bar{\boldsymbol{V}}^{(1)}_{2i-2,{\rm out}}(t) = \boldsymbol{Z}_0 \bar{\boldsymbol{I}}^{(1)}_{2i-2,{\rm out}}(t) + \boldsymbol{V}^{(0)}_{{\rm th},4i-4}(t)$$
$$\bar{\boldsymbol{V}}^{(1)}_{2i-1,{\rm in}}(t) = \boldsymbol{Z}_0 \bar{\boldsymbol{I}}^{(1)}_{2i-1,{\rm in}}(t) + \boldsymbol{V}^{(0)}_{{\rm th},4i-3}$$
$$i = 1, 2, \ldots, n_{\rm odd}. \tag{26}$$

The terminal conditions of (26) along with the equations of the corresponding lossy sections together form the set of ordinary differential equations describing the ith subcircuit of group A which can be solved for a self-consistent solution of the waveforms $\{\bar{\boldsymbol{V}}^{(1)}_{2i-2,{\rm out}}(t), \bar{\boldsymbol{V}}^{(1)}_{2i-1,{\rm in}}(t)\}$. Once the GJ is concluded, the voltage waveforms $\{\bar{\boldsymbol{V}}^{(1)}_{2i-2,{\rm out}}(t), \bar{\boldsymbol{V}}^{(1)}_{2i-1,{\rm in}}(t)\}$ determined from the present iteration of group A are used to update the relaxation sources $\{\boldsymbol{V}^{(1)}_{{\rm th},4i-5}(t), \boldsymbol{V}^{(1)}_{{\rm th},4i-2}(t)\}, i = 1, 2, ..., n_{\rm even}$, which are responsible for exciting only the even numbered subcircuits (group B) using (23) as

$$V^{(1,j)}_{{\rm th},4i-5}(t) = 2\bar{V}^{(1,j)}_{2i-2,{\rm out}}(t-\tau_j) - W^{(0,j)}_{4i-4}(t-\tau_j) + V^{(j)}_{4i-5,x}(t)$$
$$V^{(1,j)}_{{\rm th},4i-2}(t) = 2\bar{V}^{(1,j)}_{2i-1,in}(t-\tau_j) - W^{(0,j)}_{4i-3}(t-\tau_j) - V^{(j)}_{4i-2,x}(t)$$
$$j = 1, ..., m. \tag{27}$$

In (27), the first superscript refers to the iteration count while j is the line number. It is appreciated that solving the $2mn_{\rm odd}$ linear algebraic equation of (27) does not require any matrix inversion and can be solved at a significantly smaller computational cost than that of solving any subcircuit. Moreover, the $2mn_{\rm odd}$ equations of (27) being decoupled can be solved in parallel. Using the value of $\{\boldsymbol{V}^{(1)}_{{\rm th},4i-5}(t), \boldsymbol{V}^{(1)}_{{\rm th},4i-2}(t)\}, i = 1, 2, ..., n_{\rm even}$, from (27) translates to the following terminal conditions for the ith subcircuit in group B:

$$\bar{\boldsymbol{V}}^{(1)}_{2i-2,{\rm in}}(t) = \boldsymbol{Z}_0 \bar{\boldsymbol{I}}^{(1)}_{2i-2,{\rm in}}(t) + \boldsymbol{V}^{(1)}_{{\rm th},4i-5}(t)$$
$$\bar{\boldsymbol{V}}^{(1)}_{2i-1,{\rm out}}(t) = \boldsymbol{Z}_0 \bar{\boldsymbol{I}}^{(1)}_{2i-1,{\rm out}}(t) + \boldsymbol{V}^{(1)}_{{\rm th},4i-2},\ i = 1, 2, \ldots, n_{\rm even}. \tag{28}$$

The terminal conditions of (28) along with the equations of the corresponding lossy sections together form the set of ordinary differential equations describing the ith subcircuit of group B which can be solved for a self-consistent solution of the waveforms $\{\bar{\boldsymbol{V}}^{(1)}_{2i-2,{\rm in}}(t), \bar{\boldsymbol{V}}^{(1)}_{2i-1,{\rm out}}(t)\}$. These known waveforms can now be used to update the waveforms $\{\boldsymbol{V}^{(1)}_{{\rm th},4i-4}(t),\ \boldsymbol{V}^{(1)}_{{\rm th},4i-3}(t)\}$ which are responsible for exciting only the odd numbered subcircuits (group A) using (23) as

$$V^{(1,j)}_{{\rm th},4i-3}(t) = 2\bar{V}^{(1,j)}_{2i-1,{\rm out}}(t-\tau_j) - W^{(1,j)}_{4i-2}(t-\tau_j) + V^{(j)}_{4i-3,x}(t)$$
$$V^{(1,j)}_{{\rm th},4i-4}(t) = 2\bar{V}^{(1,j)}_{2i-2,{\rm in}}(t-\tau_j) - W^{(1,j)}_{4i-5}(t-\tau_j) - V^{(j)}_{4i-4,x}(t)$$
$$j = 1, ..., m. \tag{29}$$

The total $2mn_{\rm even}$ equations of (29) can be solved efficiently in parallel as well. The aforementioned iterative cycle continues till the absolute error of the iterations satisfies the error tolerance as

$$\varepsilon = \frac{1}{2n}\sum_{j=1}^{m}\sum_{i=1}^{2n}\left|V^{(k+1,j)}_{{\rm th},i} - V^{(k,j)}_{{\rm th},i}\right| \le \eta. \tag{30}$$

It is observed that the hybrid iterative technique offers twice as much as information exchange using (27) and (29) compared to the single exchange of information in traditional GJ [15]. In the next section, a methodology that exploits the delay extraction feature of DEPACT to provide an improved initial guess $\{\boldsymbol{V}^{(0)}_{{\rm th},i}(t)\}, i = 1, \ldots, n$, is described.

C. Improving the Initial Guess Based on Delay Extraction

In this section, a technique to improve the initial guess of the relaxation sources based on the delay extraction of the DEPACT model and time windowing is explained. It is noted that while time windowing, in itself, can be used to accelerate convergence [15], in this study it provides an additional benefit of reusing the data from previous time windows to obtain an improved guess of the waveforms in the present time window.

This methodology begins by dividing the entire time of interest $[0 - T]$ into μ uniform windows as $\{[0 - T_1], [T_1 - T_2], ..., [T_{\mu-1} - T]\}$ and performing the hybrid iterations of Section III-B sequentially for each time window. Considering any $[T_a - T_{a+1}]$time window, instead of a blind initial guess, the improved initial guess of $\{\boldsymbol{V}^{(0)}_{{\rm th},4i-4}(t), \boldsymbol{V}^{(0)}_{{\rm th},4i-3}(t)\}$,

$i = 1, 2, ..., n_{\text{odd}}$, can be formulated using (29) as

$$V_{\text{th},4i-3}^{(0,j)}(t) = 2\bar{V}_{2i-1,\text{out}}^{(j)}(t-\tau_j) - W_{4i-2}^{(j)}(t-\tau_j) + V_{4i-3,x}^{(j)}(t)$$
$$V_{\text{th},4i-4}^{(0,j)}(t) = 2\bar{V}_{2i-2,\text{in}}^{(j)}(t-\tau_j) - W_{4i-5}^{(j)}(t-\tau_j) - V_{4i-4,x}^{(j)}(t)$$
$$T_a < t \le T_a + \tau_j \qquad (31)$$

and

$$V_{\text{th},4i-4}^{(0,j)}(t) = V_{\text{th},4i-3}^{(0,j)}(t) = 0; \quad T_a + \tau_j < t \le T_{a+1}. \quad (32)$$

It is observed that the right-hand side (RHS) of (31) is obtained from the solution of group B for the previous time window $[T_{a-1} - T_a]$ which has already reached convergence (hence the superscripts denoting their iteration counts are dropped). As a result, $\{V_{\text{th},4i-4}^{(0,j)}(t), V_{\text{th},4i-3}^{(0,j)}(t)\}$ matches its exact waveforms $\{V_{\text{th},4i-4}^{(j)}(t), V_{\text{th},4i-3}^{(j)}(t)\}$ for $T_a < t \le T_a + \tau_j$ prior to any iteration. Using the improved waveforms of (31) and (32) into (26), the subcircuits of group A can be solved for the present $[T_a - T_{a+1}]$ window. Since the choice of the relaxation sources matches their exact waveforms for $T_a < t \le T_a + \tau_j$, the solution of group A $\{\bar{\boldsymbol{V}}_{2i-2,\text{out}}^{(1)}(t), \bar{\boldsymbol{V}}_{2i-1,\text{in}}^{(1)}(t)\}$ is guaranteed to exactly match its actual solution $\{\bar{\boldsymbol{V}}_{2i-2,\text{out}}(t), \bar{\boldsymbol{V}}_{2i-1,\text{in}}(t)\}$ for the same $T_a < t \le T_a + \tau_j$ after the first iteration of group A.

Similarly, the sources $\{\boldsymbol{V}_{\text{th},4i-5}^{(0,j)}(t), \boldsymbol{V}_{\text{th},4i-2}^{(0,j)}(t)\}, i = 1, 2, ..., n_{\text{even}}$, exciting the subcircuits of group B can be updated using (27) as

$$V_{\text{th},4i-5}^{(1,j)}(t) = 2\bar{V}_{2i-2,\text{out}}^{(j)}(t-\tau_j) - W_{4i-4}^{(j)}(t-\tau_j) + V_{4i-5,x}^{(j)}(t)$$
$$V_{\text{th},4i-2}^{(1,j)}(t) = 2\bar{V}_{2i-1,\text{in}}^{(j)}(t-\tau_j) - W_{4i-3}^{(j)}(t-\tau_j) - V_{4i-2,x}^{(j)}(t)$$
$$T_a < t \le T_a + \tau_j \qquad (33)$$

and

$$V_{\text{th},4i-5}^{(1,j)}(t) = 2\bar{V}_{2i-2,\text{out}}^{(1,j)}(t-\tau_j) - W_{4i-4}^{(0,j)}(t-\tau_j) + V_{4i-5,x}^{(j)}(t)$$
$$V_{\text{th},4i-2}^{(1,j)}(t) = 2\bar{V}_{2i-1,\text{in}}^{(1,j)}(t-\tau_j) - W_{4i-3}^{(0,j)}(t-\tau_j) - V_{4i-2,x}^{(j)}(t)$$
$$T_a + \tau_j < t \le T_{a+1}. \quad (34)$$

Similar to (31), the RHS of (33) can be obtained from the previous window which has already reached convergence. Moreover, for the time span $T_a + \tau_j < t \le T_{a+1} + 2\tau_j$, the RHS of (34) already matches their exact corresponding waveforms from the present solution of group A. Hence, the solution of group B $\{\bar{\boldsymbol{V}}_{2i-2,\text{in}}^{(1)}(t), \bar{\boldsymbol{V}}_{2i-1,\text{out}}^{(1)}(t)\}$ is guaranteed to exactly match its actual solution $\{\bar{\boldsymbol{V}}_{2i-2,\text{in}}(t), \bar{\boldsymbol{V}}_{2i-1,\text{out}}(t)\}$ for the time span $T_a < t \le T_{a+1} + 2\tau_j$ after just one iteration of group B. Hereafter, proceeding with the rest of the iterations using (26)–(30) will ensure that the hybrid iterations will converge rapidly. It is noted that for the first time window $[0 - T_1]$, assuming that the MTLs were initially unexcited, an initial guess of $\{\boldsymbol{V}_{\text{th},4i-4}^{(0)}(t), \boldsymbol{V}_{\text{th},4i-3}^{(0)}(t)\}, i = 1, 2, ..., n_{\text{odd}}$ (for group A) is taken as zero.

In quantifying the computational costs of the proposed WR algorithms, it is known that the scalability of the algorithm refers to the dependence of the computational costs with size of network (i.e., number of DEPACT sections n in (10) and the number of available processors). Irrespective of the kind of structure considered, the computational costs of full blown EMI analysis of an MTL network using commercial circuit simulators like SPICE scale superlinearly as $O(n^\alpha)$ where $1.5 \le \alpha \le 2$ depending on the sparsity of the MNA matrices. On the other hand, the proposed algorithm solves the subcircuits separately and the associated costs scale only linearly $(O(n))$ leading to significant speed up over full blown SPICE EMI analysis as shown in [27]. This advantage in computational cost is applicable for any MTL structure whether printed circuit board (PCB) structures or long cables. In fact, the larger the distributed network, the more the number of DEPACT segments (n) and greater will be the provided efficiency over full blown EMI analysis like [13] and is demonstrated in Example 3.

IV. Numerical Examples

Three examples are presented in this section to demonstrate the validity and efficiency of the proposed work. For a fair comparison of the proposed LP-WR algorithm with full blown SPICE EMI simulation using segmentation techniques, this work is compared with the DEPACT model of [13] (hereafter referred to as "full EMI") which is based on a delay extraction principle and hence is highly efficient for modeling long MTL networks [28]. Both techniques are performed using MATLAB 2011b on a UNIX server (66 GB RAM and 160 GB memory). All transient simulations involve backward Euler integration method combined with sparse matrix LU factorization and forward/backward substitution [34], [35]. In all the examples provided, the nonlinear inverter terminating the networks has been synthesized using lumped circuit elements where the nonlinear behavior of the lumped elements is explicitly defined in [37]. It is assumed that the inverters do not suffer from EMI which is consistent with similar assumptions in [10]–[13], and [18].

Example 1: The objective of this example is to demonstrate the accuracy of the proposed LP-WR algorithm compared to the full EMI simulation. For this example, a three-coupled microstrip structure with the physical geometry as shown in Fig. 5(a) is considered. The p.u.l. parameters for this example are extracted from the HSPICE field solver [36] and are as follows:

$$\boldsymbol{R} = \text{diag}(6.79)\Omega/\text{m}$$
$$\boldsymbol{L} = \begin{bmatrix} 563.53 & 241.75 & 134.50 \\ 241.75 & 556.20 & 241.75 \\ 134.50 & 241.75 & 563.53 \end{bmatrix} \text{nH/m}$$
$$\boldsymbol{C} = \begin{bmatrix} 58.30 & -19.05 & -2.31 \\ -19.05 & 65.06 & -19.05 \\ -2.31 & -19.05 & 58.30 \end{bmatrix} \text{pF/m}$$
$$\boldsymbol{R}_s = \begin{bmatrix} 1.34 & -2.68e-3 & -0.11 \\ -2.68e-3 & 1.42 & -2.68e-3 \\ -0.11 & -2.68e-3 & 1.34 \end{bmatrix} \text{m}\Omega/\text{m}\sqrt{\text{Hz}}$$
$$\boldsymbol{G} = \boldsymbol{0}$$

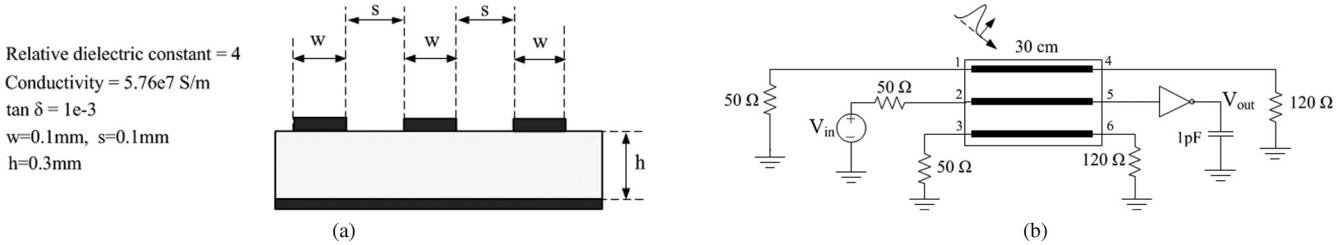

Fig. 5. Three coupled microstrip lines of Example 1. (a) Geometry of the transmission lines. (b) Circuit layout of the transmission lines.

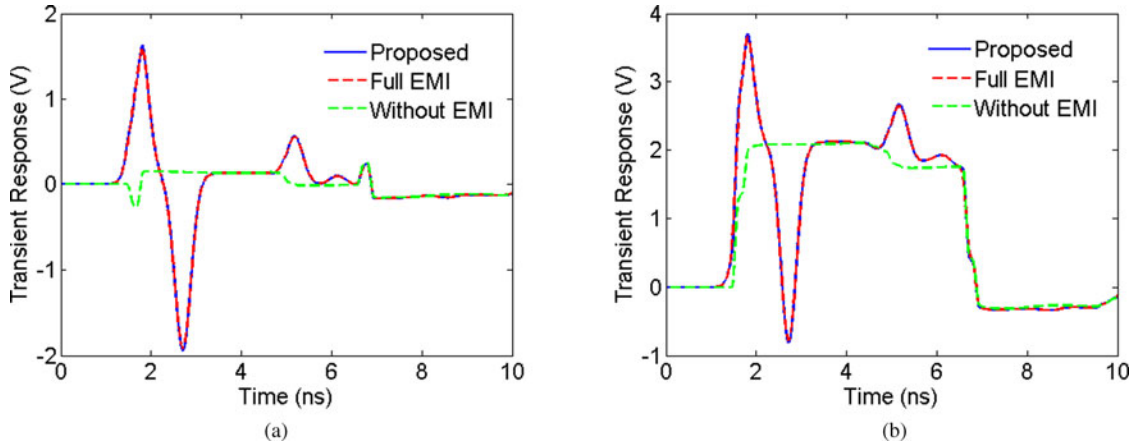

Fig. 6. Transient response for Example 1 using the proposed LP-WR algorithm and full simulation. (a) Transient response at output port 4. (b) Transient response at output port 5.

where $\boldsymbol{R}_t(s) = \boldsymbol{R}_s\sqrt{f}(1+j)$ represents the skin effect losses as a function of frequency f [36] and *diag* refers to a diagonal matrix. For the following analysis, the line length of the network is set to $l = 30$ cm. In this case, the number of subcircuits required for the proposed LP-WR is $n = 50$. The network is excited by a trapezoidal voltage source of rise time $T_r = 0.1$ ns, pulse width $T_p = 5$ ns, and an amplitude of 1.8 V, and loaded with a nonlinear inverter [37] as shown in Fig 5(b). This network is also exposed to an incident electric field with Gaussian temporal waveform $E(t) = E_0(\exp((t-t_0)^2/T^2))$ where $t_0 = 1$ ns and $T = 0.25$ ns, the peak amplitude $E_0 = 5$ kV/m, an elevation angle $\theta_p = 60°$, azimuthal angle $\varphi_p = -60°$, and a polarized angle $\theta_E = -90°$ as in Fig. 1.

To illustrate the accuracy of the proposed algorithm, the network is solved using two methods—the hybrid iterative technique with improved initial guess and the full EMI simulation [13]. For the hybrid technique, the entire time span of analysis between 0 and 10 ns is divided into 20 time windows and the iterations for each time window are performed on a sequential platform (one processor). For a predefined error tolerance of $\eta = 1e-5$, the hybrid technique required five iterations to converge. The transient responses at the far end of the network using the proposed work are illustrated in Fig. 6 and exhibit good agreement with the full EMI simulation. Fig. 7 shows the response of the output of the inverter (V_{out}) illustrating the false switching induced due to the incident field. The CPU cost of solving the full network (full EMI simulation) is 364 s and the CPU cost of the proposed LP-WR is 89 s (speedup of four times).

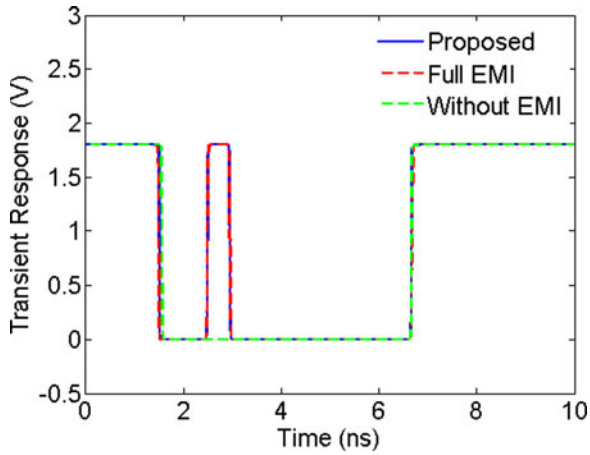

Fig. 7. Transient response (V_{out}) of an inverter in Example 1 with incident fields.

Example 2: The objective of this example is to illustrate the convergence properties of the hybrid iterative technique with improved initial guess. For this example, a three-coupled line network with the physical dimensions as shown in Fig. 8(a) is considered. The p.u.l. parameters for this example are extracted from the HSPICE field solver [36] and are as follows:

$$\boldsymbol{R} = \text{diag}(14.47)\Omega/\text{m}$$

$$\boldsymbol{L} = \begin{bmatrix} 596.07 & 188.24 & 129.51 \\ 188.24 & 560.18 & 181.65 \\ 129.51 & 181.65 & 559.07 \end{bmatrix} \text{ nH/m}$$

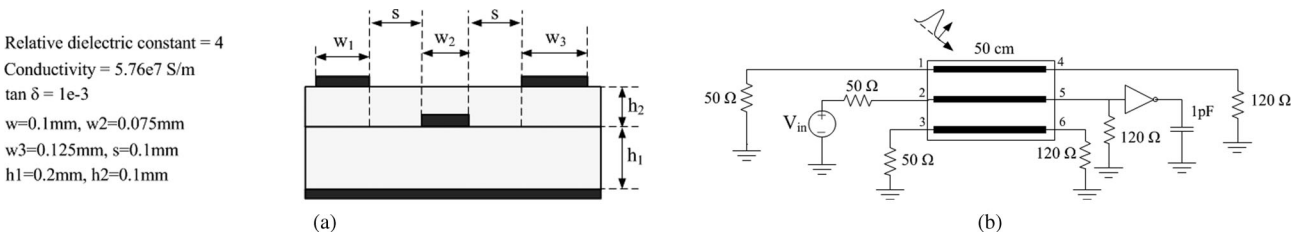

Fig. 8. MTL structure of Example 2. (a) Geometry of the transmission lines. (b) Circuit layout of the transmission lines.

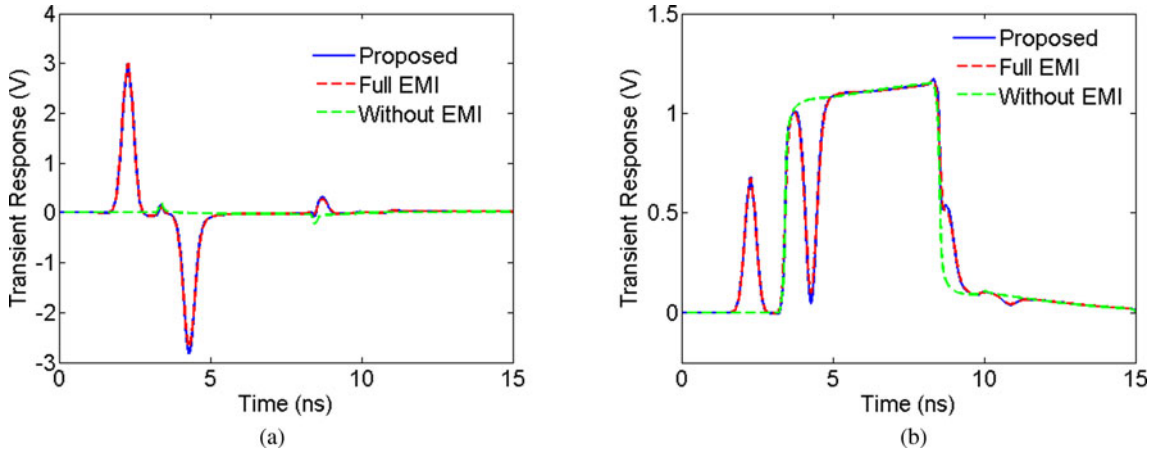

Fig. 9. Transient response for Example 2 using the proposed LP-WR algorithm and full simulation. (a) Transient response at output port 4. (b) Transient response at output port 5.

$$\boldsymbol{C} = \begin{bmatrix} 82.22 & -25.33 & -12.28 \\ -25.33 & 95.86 & -25.99 \\ -12.28 & -25.99 & 87.32 \end{bmatrix} \text{ pF/m}$$

$$\boldsymbol{R}_s = \begin{bmatrix} 1.87 & -0.24 & -0.13 \\ -0.24 & 2.33 & -0.23 \\ -0.13 & -0.23 & 1.58 \end{bmatrix} \text{ m}\Omega/\text{m}\sqrt{\text{Hz}}$$

$$\boldsymbol{G} = \boldsymbol{0}$$

where $\boldsymbol{R}_t(s) = \boldsymbol{R}_s\sqrt{f}(1+j)$ represents the skin effect losses as a function of frequency f [36]. The line length of the network is set to $l = 50$ cm which requires $n = 80$ subcircuits for the proposed LP-WR algorithm. The circuit network topology is shown in Fig. 8(b) where line 2 is excited with trapezoidal voltage sources of rise time $T_r = 0.1$ ns, pulse width $T_p = 5$ ns, and an amplitude of 1.8 V, and terminated with a nonlinear inverter [37]. This network is exposed to the same Gaussian incident electric field as Example 1.

To illustrate the accuracy of the proposed work, the network is solved using two methods—the hybrid iterative technique with improved initial guess and the full EMI simulation [13]. For the hybrid technique, the entire time span of analysis between 0 and 15 ns is divided into 20 time windows and the iterations for each time window are performed on a sequential platform (one processor). For a predefined error tolerance of $\eta = 1e-5$, the hybrid technique required four iterations to converge. The transient responses at the far end of the network using the proposed work are shown to exhibit good agreement with the full EMI simulation in Fig. 9.

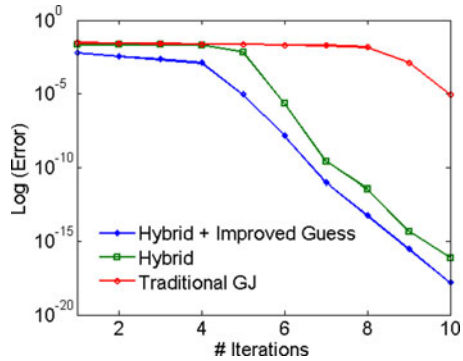

Fig. 10. Convergence properties of the proposed hybrid iterative technique compared to GJ.

Next, the convergence properties of the hybrid technique (both with and without the improved initial guess) are compared with the traditional GJ technique [15]. To perform a fair comparison, all three relaxation techniques used time windowing [15], where the entire time span of analysis between 0 and 15 ns is divided into 20 time windows and the iterations for each window are performed on a sequential platform. For the case of the hybrid technique without the improved initial guess, the initial guess is chosen as the dc solution of zero. For each technique, the number of iterations is varied from 1 to 10 and the associated error [ε of (30)] with the number of iterations is displayed in Fig. 10. It is observed that the hybrid technique

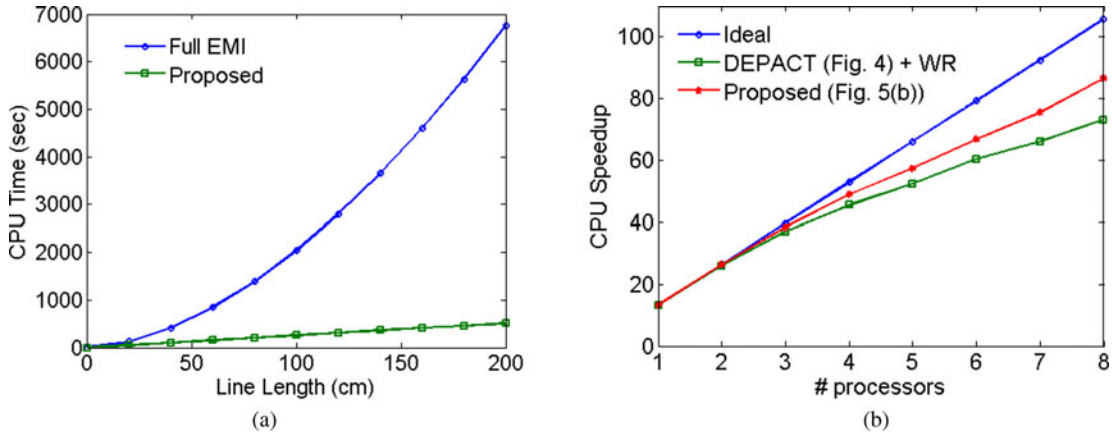

Fig. 11. Computational efficiency of the proposed LP-WR algorithm over full EMI simulation. (a) Scaling of computational cost with size of the network. (b) Scaling of computational cost with a number of parallel processors.

shows significantly faster convergence than the traditional GJ algorithms. This is due to the fact that the proposed hybrid technique involves twice the amount of information exchange as the GJ technique for same number of iterations. Moreover, when the hybrid technique is combined with an improved initial guess, it results in a further reduction of the iteration error than that of the hybrid technique with a blind initial guess.

Example 3: The objective of this example is to demonstrate the scalability of the proposed work with respect to the size of the network and the numbers of CPUs available for parallel processing. For this example, a seven-coupled microstrip structure of [27] with p.u.l. parameter matrices $\boldsymbol{R}, \boldsymbol{L}, \boldsymbol{C}, \boldsymbol{R}_s$, and $\boldsymbol{G}$ as shown at the top of the next page, where $\boldsymbol{R}_t(s) = \boldsymbol{R}_s\sqrt{f}(1+j)$ represents the skin effect losses as a function of frequency f [36]. In addition, the MTL is exposed to an incident electric field with a double exponential temporal waveform $E(t) = E_0\left(\exp\left(-\alpha t\right) - \exp\left(-\beta t\right)\right)$ with $\alpha = 4 \times 10^8$ and $\beta = 10^9$, the peak amplitude $E_0 = 1$ kV/m, an elevation angle $\theta_p = 60°$, an azimuthal angle $\varphi_p = -60°$, and a polarized angle $\theta_E = -90°$ as in Fig. 1.

This example begins with a demonstration of the scaling of the computational cost of the proposed work compared to full EMI simulation as the size of the network increases. For this purpose, the line length l of the network is increased from 0 to 200 cm in steps of 10 cm. To accurately model the network, the number n of subcircuits is increased in steps of 16 for each 10 cm step and ranges from 0 to 320. For each case, the network is solved using two methods—the proposed hybrid iterative technique with initial guess and the full EMI simulation of [13]. For the hybrid technique, the entire time span of analysis between 0 and 15 ns is divided into 20 time windows and the iterations for each time window are performed on a sequential platform. For a predefined error tolerance of $\eta = 1e-5$, the hybrid technique required on average five iterations to converge. The scaling of the computational cost of both proposed work and full EMI simulation with the line length l is shown in Fig. 11(a). It is observed from Fig. 11(a) that the proposed work scales almost linearly $(O(n))$ (as expected for the proposed LP-WR [27]) while the full EMI simulation of the original network scales superlinearly as $O(n^\alpha)$ where $\alpha \approx 1.73$ for this example.

TABLE I
CPU TIME COMPARISON FOR EXAMPLE 3

# CPU	CPU Time (sec)			Speedup w. r. t. DEPACT (Fig. 3) + WR	Speedup w. r. t. Proposed (Fig. 4b)
	DEPACT (Fig. 3) + WR	Proposed (Fig. 4b)	Full EMI		
1	511.50	511.49	6763.90	13.22	13.22
2	260.49	260.03		25.96	26.01
4	148.49	140.44		45.55	48.16
6	111.80	102.25		60.50	66.15
8	95.55	80.65		70.78	83.86

Next, the performance of the proposed work is demonstrated on a parallel platform. For this purpose, the length of the network is fixed at the corner of our design space where $l = 200$ cm. The network is solved using three methods—full EMI simulation [13], the hybrid technique with initial guess where the partitioning is performed directly on the circuit of Fig. 3, and the same hybrid technique when the partitioning is performed on the more compact circuit of Fig. 4(b). Both hybrid techniques use the same time windowing as above and the iterations for each time window are performed on a parallel platform where the number of available CPUs is varied from $p = 1$ to $p = 8$ and the error tolerance sets to $\eta = 1e-5$. The scaling of the CPU speedup offered by the proposed hybrid techniques over full EMI simulations as a function of the number of processors is shown in Fig. 11(b) and summarized in Table I. As expected, the speedup for both techniques scales efficiently with the number of processors. However, when the partitioning is performed on the circuit of Fig. 4(b), the resultant savings in the size of the subcircuits and the communication overheads lead to a more improved scaling of the CPU speedup (closer to the ideal scenario where it is assumed that no communication or scheduling overheads are incurred) than that using the circuit of Fig. 3 without Thevenin's representation.

$$\boldsymbol{R} = \text{diag}(3.82)\ \Omega/\text{m}$$

$$\boldsymbol{L} = \begin{bmatrix} 357.87 & 75.78 & 25.33 & 11.39 & 6.25 & 3.93 & 2.72 \\ 75.78 & 353.93 & 74.80 & 24.99 & 11.24 & 6.19 & 3.93 \\ 25.33 & 74.80 & 353.67 & 74.71 & 24.96 & 11.24 & 6.25 \\ 11.39 & 24.99 & 74.71 & 353.64 & 74.71 & 24.99 & 11.39 \\ 6.25 & 11.24 & 24.96 & 74.71 & 353.67 & 74.80 & 25.33 \\ 3.93 & 6.19 & 11.24 & 24.99 & 74.80 & 353.93 & 7.78 \\ 2.72 & 3.93 & 6.25 & 11.39 & 25.33 & 75.78 & 357.87 \end{bmatrix} \text{nH/m}$$

$$\boldsymbol{C} = \begin{bmatrix} 100.69 & -10.70 & -0.73 & -0.30 & -0.17 & -0.11 & -0.08 \\ -10.70 & 102.34 & -10.61 & -0.69 & -0.28 & -0.16 & -0.11 \\ -0.73 & -10.61 & 102.34 & -10.60 & -0.69 & -0.28 & -0.17 \\ -0.30 & -0.69 & -10.60 & 102.34 & -10.60 & -0.69 & -0.30 \\ -0.17 & -0.28 & -0.69 & -10.60 & 102.34 & -10.61 & 25.33 \\ -0.11 & -0.16 & -0.28 & -0.69 & -10.61 & -0.73 & -10.70 \\ -0.08 & -0.11 & -0.17 & -0.30 & -0.73 & -10.70 & 100.69 \end{bmatrix} \text{pF/m}$$

$$\boldsymbol{R}_s = \begin{bmatrix} 0.88 & -0.005 & -0.008 & 0.002 & 0.005 & 0.005 & 0.004 \\ -0.005 & 0.92 & 0.008 & -0.004 & 0.004 & 0.006 & 0.005 \\ -0.008 & 0.008 & 0.92 & 0.008 & -0.003 & 0.004 & 0.005 \\ 0.002 & -0.004 & 0.008 & 0.92 & 0.008 & -0.004 & 0.002 \\ 0.005 & 0.004 & -0.003 & 0.008 & 0.92 & 0.008 & 0.008 \\ 0.005 & 0.006 & 0.004 & -0.004 & 0.008 & 0.92 & -0.005 \\ 0.004 & 0.005 & 0.005 & 0.002 & 0.008 & -0.005 & 0.88 \end{bmatrix} \text{m}\Omega/\text{m}\sqrt{\text{Hz}}$$

$$\boldsymbol{G} = \boldsymbol{0}$$

V. Conclusion

In this paper, a longitudinal partitioning-based WR algorithm for efficient EMI analysis of MTL networks is presented. Typically, the longitudinal partitioning-based WR algorithm suffered from slow convergence due to the application of Dirichlet's transmission condition between subcircuits. In the proposed work, an improved partitioning technique is proposed that replaces Dirichlet's transmission conditions with delayed linear equations thereby accelerating the convergence of the WR iterations. Moreover, the subcircuits are solved independently using a hybrid iterative technique that combines the fast convergence of the proposed GS technique with the parallelizability of the GJ technique. Techniques to compress the size of the subcircuits and reduce communication overheads are also provided. The proposed algorithm is found to scale only linearly with the size of the network and naturally lends itself for parallel implementations.

References

[1] R. Achar and M. Nakhla, "Simulation of high-speed interconnects," *Proc. IEEE*, vol. 89, no. 5, pp. 693–728, May 2001.

[2] C. R. Paul, *Analysis of Multiconductor Transmission Line*. New York, 2008.

[3] C. R. Paul, "A SPICE model for multiconductor transmission lines excited by an incident electromagnetic field," *IEEE Trans. Electromagn. Compat.*, vol. 36, pp. 342–354, Nov. 1994.

[4] C. R. Paul, "Literal solutions for the time-domain response of a two-conductor transmission line excited by an incident electromagnetic field," *IEEE Trans. Electromagn. Compat.*, vol. 37, no. 2, pp. 241–251, May 1995.

[5] I. Maio and F. Canavero, "Analysis of crosstalk and field coupling to lossy MTLs in a SPICE environment," *IEEE Trans. Electromagn. Compat.*, vol. 38, no. 3, pp. 221–229, Aug. 1996.

[6] Y. Kami and R. Sato, "Circuit-concept approach to externally excited transmission lines," *IEEE Trans. Electromagn. Compat.*, vol. EMC-27, no. 4, pp. 177–183, Nov. 1985.

[7] P. Bernardi, R. Cicchetti, and C. Pirone, "Transient response of a microstrip line circuit excited by an external electromagnetic source," *IEEE Trans. Electromagn. Compat.*, vol. 34, no. 2, pp. 100–108, May 1992.

[8] I. Wuyts and D. Zutter, "Circuit model for plane-wave incidence on multiconductor transmission lines," *IEEE Trans. Electromagn. Compat.*, vol. 36, no. 3, pp. 206–212, Aug. 1994.

[9] R. K. Das and W. T. Smith, "Incident field coupling analysis of multiconductor transmission lines using asymptotic waveform evaluation," in *Proc. IEEE Int. Symp. Electromagnetic Compatibility*, Aug. 1996, pp. 265–270.

[10] I. Erdin, R. Khazaka, and M. Nakhla, "Simulation of high-speed interconnects in a multilayered medium in the presence of incident field," *IEEE Trans. Microw. Theory Tech.*, vol. 46, no. 12, pp. 2251–2257, Dec. 1998.

[11] I. Erdin, A. Dounavis, R. Achar, and M. Nakhla, "A SPICE model for incident field coupling to lossy multiconductor transmission lines," *IEEE Trans. Electromagn. Compat.*, vol. 43, no. 4, pp. 485–494, Nov. 2001.

[12] G. S. Shinh, N. Nakhla, R. Achar, M. Nakhla, A. Dounavis, and I. Erdin, "Fast transient analysis of incident field coupling to multiconductor transmission lines," *IEEE Trans. Electromagn. Compat.*, vol. 48, no. 1, pp. 57–73, Nov. 2006.

[13] G. Shinh, R. Achar, N. Nakhla, M. Nakhla, and I. Erdin, "Simplified macromodel of MTLs with incident fields (SiMMIF)," *IEEE Trans. Electromagn. Compat.*, vol. 50, no. 2, pp. 375–389, May 2008.
[14] E. Lelarasmee, A. E. Ruehli, and A. L. Sangiovanni-Vincentelli, "The waveform relaxation method for time-domain analysis of large-scale integrated circuits," *IEEE Trans. Comput.-Aided Design Integr. Circuits Syst.*, vol. 1, no. 3, pp. 131–145, Jul. 1982.
[15] J. White and A. L. Sangiovanni-Vincentelli, *Relaxation Techniques for the Simulation of VLSI Circuits*. Norwell, MA: Kluwer, 1987.
[16] N. M. Nakhla, A. E. Ruehli, R. Achar, and M. S. Nakhla, "Simulation of coupled interconnects using waveform relaxation and transverse partitioning," *IEEE Trans. Adv. Packag.*, vol. 29, no. 1, pp. 78–87, Feb. 2006.
[17] N. Nakhla, A. E. Ruehli, M. S. Nakhla, R. Achar, and C. Chen, "Waveform relaxation techniques for simulation of coupled interconnects with frequency-dependent parameters," *IEEE Trans. Adv. Packag.*, vol. 30, no. 2, pp. 257–269, May 2007.
[18] A. R. Sridhar, N. M. Nakhla, R. Achar, M. S. Nakhla, and A. E. Ruehli, "Fast EMI analysis via transverse partitioning and waveform relaxation," *IEEE Trans. Electromagn. Compat.*, vol. 51, no. 2, pp. 358–371, May 2009.
[19] D. Paul, N. M. Nakhla, R. Achar, and M. S. Nakhla, "Parallel simulation of massively coupled interconnect networks," *IEEE Trans. Adv. Packag.*, vol. 33, no. 1, pp. 115–127, Feb. 2010.
[20] R. Achar, M. S. Nakhla, H. S. Dhindsa, A. R. Sridhar, D. Paul, and N. M. Nakhla, "Parallel and scalable transient simulator for power grids via waveform relaxation (PTS-PWR)," *IEEE Trans. Very Large Scale Integr. (VLSI) Systs.*, vol. 19, no. 2, pp. 319–332, Feb. 2011.
[21] F. Y. Chang, "The generalized method of characteristics for waveform relaxation analysis of lossy coupled transmission lines," *IEEE Trans. Microw. Theory Tech.*, vol. 37, no. 12, pp. 2028–2038, Dec. 1989.
[22] F. Y. Chang, "Waveform relaxation analysis of RLCG transmission lines," *IEEE Trans. Circuits Syst.*, vol. 37, no. 11, pp. 1394–1415, Nov. 1990.
[23] F. Y. Chang, "Relaxation simulation of transverse electromagnetic wave propagation in coupled transmission lines," *IEEE Trans. Circuits Syst.*, vol. 38, no. 8, pp. 916–936, Aug. 1991.
[24] F. Y. Chang, "Waveform relaxation analysis of nonuniform lost transmission lines characterized with frequency dependent parameters," *IEEE Trans. Circuits Syst.*, vol. 38, no. 12, pp. 1484–1500, Dec. 1991.
[25] F. Y. Chang, "Transient simulation of nonuniform coupled lossy transmission lines characterized with frequency-dependent parameters: Part I. Waveform relaxation analysis," *IEEE Trans. Circuits Syst. I, Fundam. Theory Appl.*, vol. 39, no. 8, pp. 585–603, Aug. 1992.
[26] M. Al-Khaleel, A. E. Ruehli, and M. J. Gander, "Optimizedwaveform relaxation methods for longitudinal partitioning of transmission lines," *IEEE Trans. Circuits Syst. I, Reg. Papers*, vol. 56, no. 9, pp. 1732–1743, Aug. 2009.
[27] S. Roy and A. Dounavis, "Longitudinal-partitioning-based waveform relaxation for efficient analysis of distributed transmission-lines," *IEEE Trans. Microw. Theory Tech.*, vol. 60, no. 3, pp. 451–463, Mar. 2012.
[28] N. Nakhla, A. Dounavis, R. Achar, and M. S. Nakhla, "DEPACT: Delay extraction-based passive compact transmission-line macromodeling algorithm," *IEEE Trans. Adv. Packag.*, vol. 28, no. 1, pp. 13–23, Feb. 2005.
[29] N. Nakhla, M. S. Nakhla, and R. Achar, "Simplified delay extraction-based passive transmission line macromodeling algorithm," *IEEE Trans. Adv. Packag.*, vol. 33, no. 2, pp. 498–509, May 2010.
[30] F. H. Branin, Jr., "Transient analysis of lossless transmission lines," *Proc. IEEE*, vol. 55, no. 11, pp. 2012–2013, Nov. 1967.
[31] F. Fer, "Resolution de l'equation matricielled U/dt = pU par produit infini d'exponentielles matricielles," *Acad. R. Belg. Cl. Sci.*, vol. 44, no. 5, pp. 818–829, 1958.
[32] J. D. Dixon, "Exact solution of linear equations using p-adic expansions," *Numer. Math.*, vol. 40, no. 1, pp. 137–141, 1982.
[33] W. Eberly, M. Giesbrecht, P. Giorgi, A. Storjohann, and G. Villard, "Solving sparse integer linear systems," in *Proc. Int. Symp. Symbolic Algebraic Comput.*, Genova, Italy, Jul. 2006, pp. 63–70.
[34] J. Vlach and K. Singhal, *Computer Methods for Circuit Analysis and Design*. New York: Van Nostrand, 1983.
[35] T. A. Davis, *Direct Methods for Sparse Linear Systems*. Philadelphia, PA: SIAM, 2006.
[36] *HSPICE Signal Integrity User Guide,* Synopsys Inc., CA, Sep. 2005
[37] B. Toner and V. F. Fusco, "Waveform based MOSFET dynamic large signal parameter estimation," *IEE Proc. Microw., Antennas Prop.*, vol. 150, no. 6, pp. 451–458, Dec. 2003.

Sourajeet Roy (S'11) received the B.Tech. degree in electrical engineering from Sikkim Manipal University, Sikkim, India, and the M.E.Sc. degree from Western University, London, ON, Canada, in 2006 and 2009, respectively. He is currently working toward the Ph.D. degree at the Department of Electrical and Computer Engineering, Western University.

His research interests include modeling and simulation of high-speed circuits, signal and power integrity analysis of electronic packages, and design and implementation of parallel algorithms.

Mr. Roy is the recipient of the Vice-Chancellors Gold Medal at the undergraduate level in 2006, the Queen Elizabeth II Graduate Scholarship in Science and Technology, 2012, and the Ontario Graduate Scholarship, 2012.

Amir Beygi received the B.S. degree in electrical engineering from the K.N. Toosi University of Technology, Tehran, Iran, the M.S. degree in electrical engineering from the Iran University of Science and Technology, Tehran, and the Ph.D. in electrical and computer engineering from Western University, London, ON, Canada, in 2004, 2007, and 2011, respectively.

He is currently with Evertz Microsystems, Burlington, ON. His research interests include simulation and modeling algorithms for electromagnetic compatibility and signal integrity of high-speed interconnects.

Anestis Dounavis (S'00–M'03) received the B.Eng. degree from McGill University, QC, Canada, in 1995, and the M.Sc. and Ph.D. degrees from Carleton University, Ottawa, ON, in 2000 and 2004, respectively, all in electrical engineering.

He currently serves as an Associate Professor in the Department of Computer and Electrical Engineering, Western University. His research interests include electronic design automation, simulation of high-speed and microwave networks, signal integrity, and numerical algorithms.

Dr. Dounavis received the Ottawa Centre for Research and Innovation Futures Award-Student Researcher of the Year in 2004 and the INTEL Best Student Paper Award at the Electrical Performance of Electronic Packaging Conference in 2003. He also received the Carleton University Medal for outstanding graduate work at the M.Sc. and Ph.D. levels in 2000 and 2004, respectively. He also received the University Student Council Teaching Honour Roll Award at the Western University during 2009–2010.